Rich or poor: the impact of electron donation and withdrawal on the photophysical and photocatalytic properties of copper(I) complexes

Florian Doettinger, Christian Kleeberg, Clémence Queffélec, Stefanie Tschierlei, Yann Pellegrin, Michael Karnahl

ARTICLE

Rich or Poor: The Impact of Electron Donation and Withdrawal on the Photophysical and Photocatalytic Properties on Copper(I) Complexes

Received 00th January 20xx,
Accepted 00th January 20xx

DOI: 10.1039/x0xx00000x

Florian Doettinger[a], Christian Kleeberg[b], Clémence Queffélec[c], Stefanie Tschierlei[a], Yann Pellegrin[c,*] and Michael Karnahl[a,*]

Motivated by the need to design efficent photocatatalysts based on eart-abundant metals and to elucidate essential structure-property relationships this study deals with heteroleptic copper(I) complexes. A systematic series of four novel diimine-diphosphine copper(I) complexes of the type $[Cu(N^N)(P^P)]^+$ with different electron donating and withdrawing substituents in the 4,7-position of the phenanthroline moiety has been prepared and compared to those with 5,6-position. In addition, two crystal structures were obtained, including that of the important synthesis intermediate $[Cu(MeCN)_2(P^P)]^+$. Accompanying DFT calculations revealed the orbital energies and HOMO-LUMO gaps, which are strongly dependent on the substituents. Most strikingly, substitution at the 4,7-position leads to better absorption properties of the resulting complexes than in the 5,6-position. Within the series, the bistrifluoromethyl groups **$(CF_3)_2$** play a special role, *e.g.* the **Cu$(CF_3)_2$** complex is the only one that can be reduced twice. Moreover, **Cu$(CF_3)_2$** represents the strongest excited state oxidant, whose potential is shifted by 90 mV compared to the reference complex **CuH** lacking substituents. The production of reactive singlet oxygen ($^1O_2$), including the catalytic oxygenation of 2,5-diphenylfuran (DPF), as well as the photocatalytic reductive dehalogenation of arylhalides were then chosen to evaluate the activity of these complexes. In fact, all complexes are good sensitizers generating $^1O_2$ with singlet oxygen quantum yields ϕ_{1O2} of up to 54% and a DPF oxygenation efficiency that depends on the electron donation ability of the respective substituents. A screening of different substrates, including the challenging 2-chloropyridine, and catalysis parameters demonstrated that these copper(I) complexes are very potent photocatalysts for reductive dehalogenations. They enable high yields >90% and fast reactions with maximum turnover frequencies of 1180 h^{-1} (Ar-Br) and 2939 h^{-1} (Ar-I), exceeding previous benchmark complexes.

Introduction

Over the last decades, great progress has been achieved in developing more sustainable technologies. For example, organic light-emitting diodes (OLEDs)[1-4] and light-emitting electro-chemical cells (LECs)[5-7] have emerged to rival conventional approaches in the generation of light for illumination or in display technology. Also, dye-sensitized solar cells (DSSCs) for the transformation of sunlight into electricity strongly progressed.[8-11] Instead of generating electric power, light is increasingly used in photoredox catalysis to drive various chemical transformations.[12-18]

Thus, visible light has been used to drive several organic reactions with high efficiency,[13,16,19-21] such as the challenging activation of carbon-halogen bonds, in which a number of aryl and alkyl halides are converted into reactive radicals under mild conditions.[22,23] In addition to its use in organic synthesis, photocatalysis also plays an emerging role in the production of the so-called solar fuels, *e.g.* in the splitting of water to H_2 or the activation of CO_2.[24-28]

In such photocatalytic systems, coordination compounds based on transition metals are often utilized. However, as transition metals from the 2nd and 3rd row (*e.g.* Ru, Ir, Pt or Re) do not represent ideal candidates due to their low abundance in the Earth's crust, first row transition metals have gained increasing attention and already demonstrated their applicability.[27,29-33] Among the first row, copper(I) complexes show some unique properties due to its closed shell d^{10} electron configuration and the great diversity in possible ligand design.[17,31,34-39] In particular, heteroleptic diimine-diphosphine copper(I) complexes of the type $[Cu(N^N)(P^P)]^+$ (Fig. 1) came into focus due to their long excited state lifetimes, beneficial excited state potentials and broad tunability.[6,17,31,37,38,40]

[a] *Department of Energy Conversion, Institute of Physical and Theoretical Chemistry, Technische Universität Braunschweig, Rebenring 31, 38106 Braunschweig, Germany, E-mail: michael.karnahl@tu-braunschweig.de; Web: http://www.karnahl-group.de.*

[b] *Institute of Inorganic and Analytical Chemistry, Technische Universität Braunschweig, Hagenring 30, 38106 Braunschweig, Germany.*

[c] *Nantes Université, CNRS, CEISAM, UMR 6230, F-44000 Nantes, France, E-mail: yann.pellegrin@univ-nantes.fr.*

Electronic Supplementary Information (ESI) available: The ESI contains experimental, synthesis and spectroscopic details including information on photocatalysis. See DOI: xxxx

Besides rather strong variations of the ligand scaffold, by fusing additional polyaromatic rings at different positions at the phenanthroline moiety, or by attaching an additional chromophore to create bichromophoric systems,[41-46] the impact of comparably small changes with respect to electron donating[47,48] or withdrawing units[47-50] has only scarcely been studied. This, however, provides detailed insights into the structure-property relationships with presumably predictable effects on the photophysical properties and photocatalytic activity of the envisioned photosensitizer.

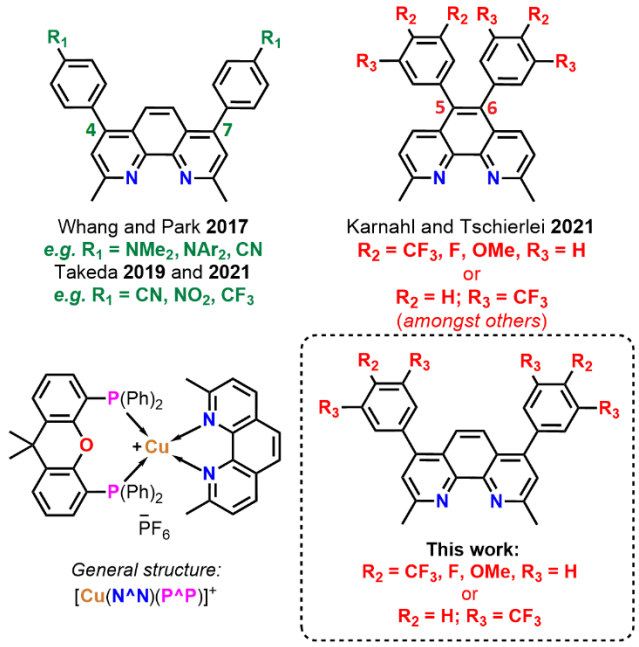

Fig. 1 Selected examples[47,49,50] of diimine ligands and the resulting heteroleptic copper(I) photosensitizers studying the impact of the various electronic functions. In our previous work[48] the effect of substitution in 5,6-position at the phenanthroline was investigated, while this study deals with the 4,7-position.

In that manner, Takeda *et al.* studied the influence of 4-nitrophenyl (NO_2) and 4-cyanophenyl (CN) introduced at the 4,7-position to 2,9-dimethyl-1,10-phenanthroline (Fig. 1).[49] Aside these derivatives, they also looked to several variations using 5-membered heteroaromatics. Their work revealed a decrease in emission lifetime and quantum yield for the investigated heteroleptic copper(I) photosensitizers (PS), when electron withdrawing groups (such as NO_2 and CN) were introduced.[49] Takeda et al. more recently also reported heteroleptic copper(I) complexes bearing trifluoromethyl (CF_3) groups. Although the emission lifetime and quantum yield were decreased for the CF_3-derivative, a higher activity for the evolution of H_2 and the photocatalytic reduction of CO_2 was found.[50] A stronger oxidative power has been suggested as a possible reason.[50] In these studies, however, no dedicated electron donating group was attached to the 4,7-diphenyl-2,9-dimethyl-1,10-phenanthroline unit (herein: **LH**, *cf.* Fig. 1 R_1 = H).

Park *et al*. studied the effect of electron poor and electron rich substituents at the 4-position of the **LH**'s phenyl substituents on the photophysical and photocatalytic properties of the resulting [Cu(**LH**)(xant)]PF_6 complexes (with xant = xantphos).[47] For this purpose, the electron rich diphenylamino- and dimethylamino-functionalized derivatives were prepared besides the electron poor cyano substituted **LH** ligand (Fig. 1). As a result, the electron donating tertiary amine lead to a much higher absorptivity and emission quantum yields, accompanied by extremely long excited state lifetimes in an aqueous tetrahydrofuran (THF) solvent mixture (THF/H_2O = 8:2 v/v).[47] In contrast, the electron withdrawing CN group caused a decrease in the same parameters, as found also by Takeda *et al*..[49] The improved photophysical properties then impressively increased the photocatalytic activity of these copper(I) PS in the light-driven reduction of water to molecular H_2.[47]

Motivated by this work, we have previously been interested in studying the effect of electron withdrawal or donation in 5,6-position at the phenanthroline scaffold (Fig. 1).[48] Therefore, we prepared and studied heteroleptic copper(I) complexes with, for example, 4-methoxyphenyl (electron donating) and 4-trifluoromethylphenyl substituents (electron withdrawing, Fig. 1). The degree of electron withdrawal or donation of a functional group can be quantified by the Hammett constant σ, with positive values for electron withdrawing groups, *e.g.* σ = +0.54 for 4-CF_3 and negative values for electron donating groups, *e.g.* σ = -0.27 for 4-OMe[51] (*cf.* Fig. 2). In our earlier study,[48] a surprisingly different behavior as would be expected from the literature was observed: the electron richest complex bearing 4-methoxyphenyl groups in 5,6-position was found to be the least absorbing with lowest excited state lifetime and weakest emission quantum yield among all the derivatives chosen.[47,49,50]

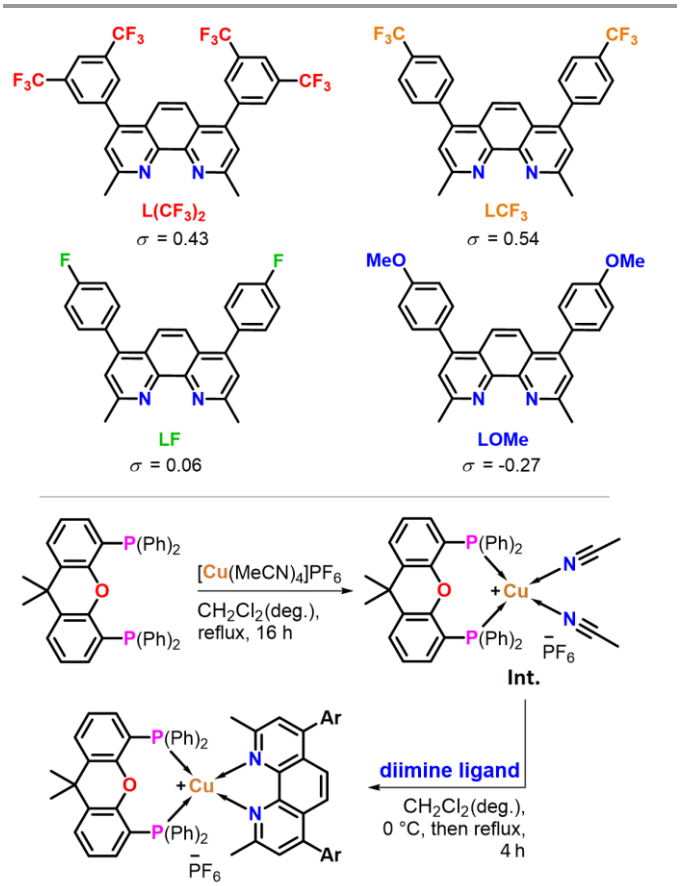

Fig. 2 Top: Representation of the four ligands **L(CF$_3$)$_2$-LOMe** in order of decreasing electron withdrawing character (top left to bottom right) together with their corresponding Hammett constants σ.[51] Bottom: General reaction route for the preparation of heteroleptic copper(I) complexes involving the intermediate [Cu(MeCN)$_2$(xant)]PF$_6$ **Int**.

To now clarify whether the very different behaviour is rooted in the variation of the position (*i.e.* 4,7- *vs.* 5,6-position) or if the chosen functional groups possess a further uncovered physical parameter, we decided to apply the same functionalization approach, but in 4,7-position of the phenanthroline (Figs. 1 and 2). This should allow for a more valid discussion about the impact of the electronic effects in 5,6- compared to the 4,7-position.

As a result of the above considerations, a systematic series of four different ligands LX, whose structure derives from **LH**, and their respective [Cu(**L**)(xant)]PF$_6$ complexes were prepared. To cover a broad range, functionalization towards the 3,5-bis-trifluoromethyl (**L(CF$_3$)$_2$**), 4-trifluoromethyl (**LCF$_3$**), 4-fluoromethyl (**LF**) and 4-methoxy (**LOMe**) derivatives (in order of declining electron withdrawing character (Fig. 2)) were chosen. Further two solid state structures were obtained and compared to theoretically predicted structures from density functional theory (DFT). The copper(I) PS were then analysed based on a combination of electrochemistry and UV/vis-, steady-state emission as well as time-resolved emission spectroscopy.

To study their capabilities as PS, the catalytic efficiencies of the compounds in the generation of singlet oxygen ($^1O_2$) were tested and compared. $^1O_2$ is used, for example, in the photodynamic therapy of cancer and in synthetic chemistry as a strong oxidant.[39,52-54] To demonstrate the applicability of the PS in this context, the catalytic photooxygenation of 2,5-diphenylfuran (DPF) to *cis*-dibenzoyl ethylene (DBE)[52,55-57] was chosen as a model reaction.

To evaluate their potential as photocatalysts, the catalytic dehalogenation of different aryl halogenides was also investigated.[22,23] To underline the high potential of these complexes, attention was given to the especially demanding dehalogenation of aryl chlorides (Scheme 1).[58-60] The dehalogenation is characterized by mild reaction conditions (blue LED light at room temperature) and short reaction times (some < 1h), which renders these heteroleptic copper(I) complexes as a new benchmark system.

Results and Discussion

Synthesis and structural characterization

Ligand synthesis (**L(CF$_3$)$_2$-LOMe**): the diimine ligands were prepared *via* Suzuki-Miyaura cross-coupling reactions from 4,7-dichloro-2,9-dimethyl-1,10-phenanthroline utilizing XPhos-Pd-G2 as catalyst. The required 4,7-dichloro-2,9-dimethyl-1,10-phenanthroline and the reactive XPhos-Pd-G2 catalyst were synthesised following literature known procedures.[61,62] Suzuki cross-coupling reactions were conducted in a biphasic THF/water mixture at reflux temperatures over 16 h (similar for all ligands). The applied optimised coupling conditions are derived from our previous study, where further details are discussed in detail.[48] The coupling reactions then proceeded quantitatively for **LCF$_3$**, **LF** and **LOMe** (98, 98 and 96%) and with a good yield for **L(CF$_3$)$_2$** (71%).

Importantly, the electron-donating derivative **LOMe** (Fig. 2) has never been reported before. The other substituted phenanthroline ligands have been presented in the literature, but for different purposes. **LCF$_3$** was prepared in a comparable reaction with the classical [Pd(PPh$_3$)$_4$] catalyst in 74% yield and employed for photocatalytic CO_2 reduction using its copper(I) complex.[50] **LF** was applied as ligand in nickel catalysed photocarboxylation reactions.[63] **L(CF$_3$)$_2$** has been incorporated into polymer solar cells, but only the sole ligand and not as a metal-containing coordination compound.[64]

Synthesis of the complexes (**Cu(CF$_3$)$_2$-CuOMe**): the respective copper(I) complexes were synthesised following a well-known one-pot two-step synthetic procedure.[48,65,66] Under inert conditions (Ar atmosphere), xantphos is introduced first, forming the [Cu(MeCN)$_2$(xant)]PF$_6$ (MeCN = acetonitrile) intermediate (**Int**), followed by fast substitution of the remaining MeCN ligands by the diimine ligand (Fig. 2). Isolated yields ranged from 75 to 85%. The four novel complexes were subsequently fully characterized by high resolution mass spectrometry as well as ^{1}H-, ^{13}C-, ^{19}F- and ^{31}P-NMR spectroscopy (see sections 3 and 4 of the ESI).

Single crystals of the **CuOMe** complex could be obtained by diffusion of *n*-heptane into a 1,2-dichloroethane solution. Moreover, for the synthesis intermediate [Cu(MeCN)$_2$(xant)]PF$_6$ (Fig. 3) single crystals of sufficient

quality for X-ray crystallography could also be isolated for the first time, even though this has been known for a long time.[40,67,68]

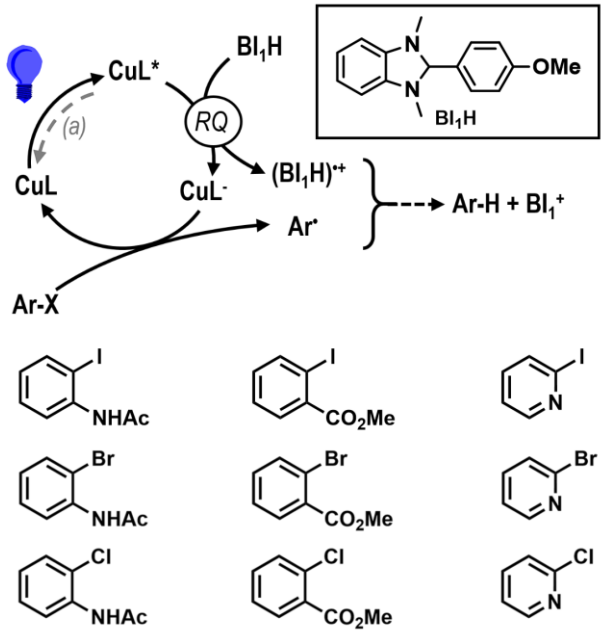

Scheme 1 Simplified reaction mechanism of the photocatalysed dehalogenation of aryl halides using copper(I) complexes as photocatalyst and BI_1H as sacrificial electron donor. The nine substrates investigated within this study are shown at the bottom.

Molecular Structure of the Synthesis Intermediate Int

As mentioned above, the solid state structure of the intermediate $[Cu(MeCN)_2(xant)]PF_6$ was determined (Fig. 3 and Table 1, **Int**), demonstrating that this complex is indeed formed as a stable compound. In this structure, the Cu-N bond lengths are significantly shortened compared to the diimine coordinated complex (Table 1), which is probably due to the sp hybridized nitrogen (compared to the sp^2 nitrogen atoms in phenanthroline). The N-Cu-N bond angle is 93.68(8)°, which is much smaller than expected for a rather undisturbed tetrahedral geometry (*i.e.* 109.5°). Most importantly, the obtained solid state structure of $[Cu(MeCN)_2(xant)]PF_6$ underlines the existence of the synthetic intermediate[40,67,68] and shows that the compound can be isolated.

Comparison between Predicted and Experimental Structures of the studied Complexes

To evaluate potential structural differences between the four copper(I) complexes, the molecular structures were calculated by DFT (B3LYP-D3(BJ)/def2-TZVP, CPCM, see ESI for details) and analysed concerning relevant changes in their bond lengths, bond and torsion angles. To ensure the validity of the predicted structures, they were compared with the solid state structure of **CuOMe** obtained by X-ray analysis (Fig. 3, Table 1 and S5.1).

In general, the experimental structure of **CuOMe** is well described by our calculations. The experimental Cu-N and Cu-P bond lengths, however, are somewhat shorter (2-4 pm) for **CuOMe**. In contrast, the C-C bond lengths and various angles between the phenanthroline moiety and the introduced methoxyphenyl substituent show no mentionable discrepancy (Table 1). The inter plane angles P-P-N-N are slightly smaller in the calculation (around 4°) compared to the experiment. The torsion angles between the phenyl ring and the phenanthroline plane are well predicted with slight differences around 5°, *e.g.* 60.10° experimentally *vs*. 55.8° on average between the five computed structures. It should also be noted that the experimental values were determined from the solid state, while the computed structures are simulated inside an implicit solvent model (CPCM in acetonitrile, *cf.* ESI). Although the computed bond lengths are slightly overestimated, the discrepancies found between theory and experiment fall within a typical error value.[69,70] Hence, with careful analysis, the computed structures have acceptable validity.

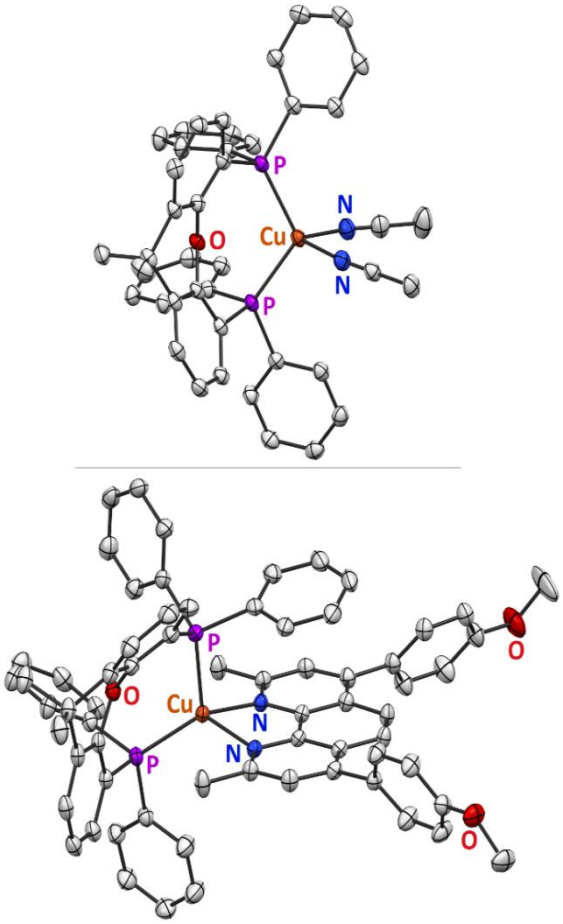

Fig. 3 Solid state molecular structure from single crystal X-ray diffraction analysis of the $[Cu(MeCN)_2(xant)]^+$ cation (**Int**, top) and the $[Cu(\mathbf{LOMe})(xant)]^+$ cation (**CuOMe**, bottom). Displacement ellipsoids are set at a probability level of 50%. Hydrogen atoms and solvent molecules are omitted for clarity.

Table 1. Selected bond lengths (pm), bond angles (°), inter plane angles (P-P-N-N, °) and torsion angles τ_{Sub} (°) of **Cu(CF$_3$)$_2$-CuOMe** and the synthesis intermediate (Int) obtained by DFT calculations and/or crystallographic analysis. The **CuOMe** complex has been analysed experimentally as well as by theory to evaluate the validity of the theoretical structures. Theoretically predicted structures are denoted as *calc.* while experimentally determined structures are denoted as *exp.*. The C-C bond lengths describe the length between the respective substituent and the phenanthroline moiety. Torsion angles τ_{Sub} express the degree of torsion between the phenanthroline plane and the plane of each substituent.

	Cu(CF$_3$)$_2$ *calc.*	CuCF$_3$ *calc.*	**CuF** *calc.*	**CuH** *calc.*	**CuOMe** *calc.*	**CuOMe** *exp.*	Int *exp.*
Cu-N	213.74	211.90	213.20	212.77	211.99	208.2(1)	204.0(2)
	214.32	213.73	213.31	213.36	213.15	210.6(1)	202.6(2)
Cu-P	227.54	226.83	226.94	226.83	226.62	224.42(6)	227.57(6)
	232.21	230.23	230.95	230.87	230.73	228.83(5)	227.61(6)
C-C	148.1	148.1	148.1	148.1	148.7	148.8(2)	/
	148.2	148.1	148.0	148.1	148.7	148.2(2)	
N-Cu-N	78.28	78.98	78.72	78.76	78.85	79.72(5)	93.68(8)
P-Cu-P	116.36	119.52	118.11	118.47	118.98	117.28(2)	112.89(2)
P-P-N-N	87.15	84.58	85.69	85.32	85.20	89.49(5)	87.00(5)
$\tau_{Sub,1}$	54.09	58.04	56.38	57.40	54.15	60.1(2)	/
$\tau_{Sub,2}$	56.40	57.03	55.98	55.57	52.23	57.6(2)	

Values given in parentheses express the estimated standard deviation of the measurement.

Trends in the DFT calculated Structures

Regarding the computed series of our functionalized copper(I) complexes, a trend can be rationalized concerning the Cu-N and Cu-P bond lengths as well as the N-Cu-N and P-Cu-P bond angles, however, with one exception. Going from the most electron withdrawing $(CF_3)_2$ functional group to the most electron donating OMe group, both, the Cu-N and Cu-P bond lengths steadily decrease with a maximum deviation of around 2 pm (Table 1). In consequence, a steady increase in the N-Cu-N and P-Cu-P bond angles and the P-P-N-N inter plane angle can be observed. This is due to the decreased donating ability of the electron deficient ligands. However, the CF_3 functionalized **CuCF$_3$** complex does not fit into this trend concerning any of the described parameters. The computed bond lengths and angles in **CuCF$_3$** must be classified as exception from the trend as no conclusive reason could be identified (the exception was yet found not to be relevant for further discussion, *vide infra*). The trend observed for the other four complexes **Cu(CF$_3$)$_2$**, **CuF**, **CuH** and **CuOMe** suggests that distal functionalization indeed affects the geometrical properties of the coordination site in a steady and reasonable manner.

Changes in Orbital Energies and HOMO-LUMO Gaps

To evaluate possible differences induced by the functional groups, the calculated structures were further analysed concerning their orbital energies (Fig. 4).[51] Notably, comparison of the highest occupied molecular orbitals (HOMOs) of the complexes revealed that their energies all lie in a quite similar regime (ΔE_{max} ≈0.08 eV, see Fig. 4: highest energies in occupied orbitals region, *e.g.* -5.6 to -5.5 eV). This small difference is reasonable, as the HOMOs in each complex are mainly characterized by a mixture of Cu-d orbitals and orbitals localized at the phosphorus atoms and the Cu-P bond (ESI Chapter 6). This is consistent with reports in the literature.[31] It is plausible that these orbitals are only slightly affected by the change of the distal substituents at the phenanthroline. Nevertheless, the still small but steady increase in the HOMO energies, when going from **Cu(CF$_3$)$_2$** to **CuOMe**, is in good agreement with the increase in bond lengths discussed above and also fits to the Hammett constants σ of the functional groups (*e.g.* σ = +0.54 or σ = -0.27, see Table 2)

Table 2. Energies of the computed HOMO-LUMO gaps Δgap of the copper(I) complexes together with the Hammett constants σ of the different substituents for comparison.[51]

	Cu(CF$_3$)$_2$	**CuCF$_3$**	**CuF**	**CuH**	**CuOMe**
Δgap [eV]	3.31	3.38	3.47	3.48	3.49
σ	+0.43*	+0.54	+0.06	0	-0.27

Note that σ refers to a single substituent in m-position, while in **Cu(CF$_3$)$_2$ the functional group is present at both possible m-positions on the phenyl substituent.*

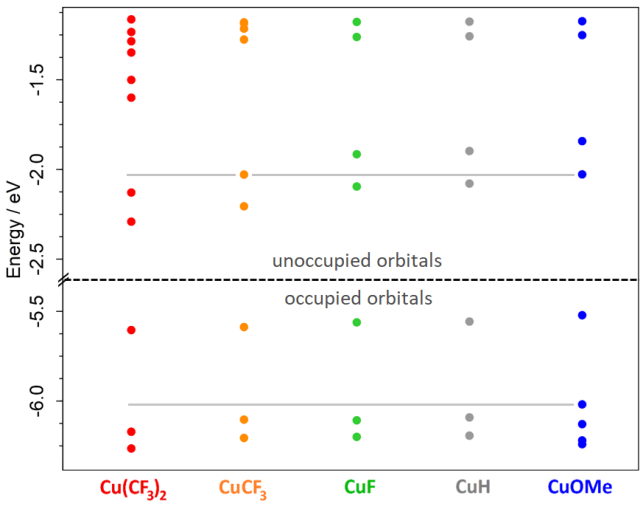

Fig. 4 Computed orbital energies of the copper(I) complexes investigated in this study. Gray solid lines are drawn to aid comparison of the respective orbital energies (drawn

for HOMO-1 and LUMO of **CuOMe**). A greater excerpt of the computed energies is depicted in the ESI Fig. S6.12.

A further interesting result from the energy analysis is obtained with regard to the lowest unoccupied molecular orbital (LUMO) and the orbital energetically just above the LUMO (termed as LUMO+1). The LUMO and LUMO+1 are both characterized by antibonding π* orbitals localized on the phenanthroline, which are significantly affected by the modification directly at the diimine (ΔE_{max} ≈0.3 eV, E = -2.3 to -2.0 eV for LUMOs and E = -2.1 to -1.8 eV or LUMOs+1). The LUMO+1 of **CuOMe** is illustrated in Fig. 5 (right plot) as a representative example (all other orbital plots of the HOMO-5 to LUMO+5 of all complexes are presented in the ESI: Chapter 6). As a main result of the different effects, the HOMO-LUMO gaps strongly vary and depend on the electronic character of the substituents. In **Cu(CF$_3$)$_2$** the gap amounts to 3.31 eV, while in **CuOMe** the gap is 3.49 eV (ΔE = 0.18 eV, Table 2).

The probably most unexpected result appears when examining the orbitals just above the mentioned LUMO and LUMO+1: both, the LUMO+2 and LUMO+3 of **Cu(CF$_3$)$_2$** lie significantly lower than those of the other complexes, where the respective orbitals are all fairly similar in energy and all lie significantly higher (Fig. 4, *e.g.* -1.6 and -1.5 eV for **Cu(CF$_3$)$_2$** *vs.* -1.3 and -1.2 eV in **CuCF$_3$**). In **Cu(CF$_3$)$_2$** these orbitals are localized on the bis(trifluoromethyl)phenyl substituents (see Fig. 5, left). In the complexes **CuCF$_3$-CuOMe** the substituent localized orbitals can be found at much higher energies (*e.g.* -0.8 to -0.5 eV in ESI Fig. S6.12).

In conclusion, from theory it can be deduced that the introduction of the $(CF_3)_2$ groups most likely causes the smallest HOMO-LUMO gap among the whole series. Furthermore, in **Cu(CF$_3$)$_2$** the energies of the substituents π* are surprisingly low. Here, the $(CF_3)_2$ functional groups decrease the energies of the substituents π* orbitals, causing them to become the LUMO+2 and LUMO+3 instead of for example the LUMO+12 in the unfunctionalized **CuH**. Both effects introduced by the $(CF_3)_2$ group should consequently lead to a less negative reduction potential (LUMO energy) and a more red-shifted absorption (HOMO-LUMO gap) in the experiment (Table 2, *vide infra*), as discussed below.

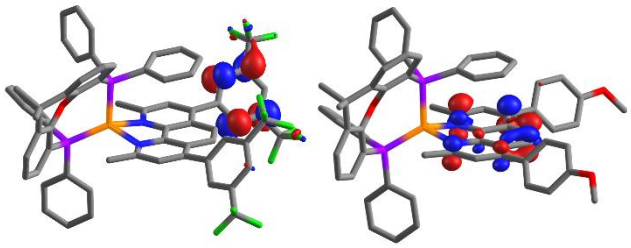

Fig. 5 Orbital representation of the LUMO+2 of **Cu(CF$_3$)$_2$** (left, E=-1.60 eV) localized on the phenyl substituent and the LUMO+1 of **CuOMe** (right, E=-1.84 eV) localized on phenanthroline.

Electrochemical studies

The novel complexes **Cu(CF$_3$)$_2$**, **CuCF$_3$**, **CuF** and **CuOMe** were further analysed *via* cyclic voltammetry in acetonitrile solution to elucidate their electrochemical behavior (ESI Figs. S7.1-4). As typical for this class of compounds and as expected from the literature-known **CuH**, all complexes possess one reversible reduction event, which is attributed to the reduction of the phenanthroline moiety (see Table 3).[40,46,48,49,71] In accordance with the theory and the work by Takeda *et al.*[49] as well as our previous study,[48] **Cu(CF$_3$)$_2$** is reduced at the most positive potential ($E_{1/2}^{red}$ = -1.85 V), while **CuOMe** is reduced at the most negative potential ($E_{1/2}^{red}$ = -2.08 V). The $E_{1/2}^{red}$ of **CuOMe** is comparable to its related complex from our prior study (Δ = 30 mV, $E_{1/2}^{red}$ = -2.11 V), which bears the same methoxyphenyl substituents in the 5,6-position instead of the 4,7-position.[48] In contrast, **Cu(CF$_3$)$_2$** shows a greater difference compared to its related 5,6-substituted compound (Δ = 90 mV, $E_{1/2}^{red}$ = -1.94 V).[48] These findings already suggest that the substitution in 4,7-position induces a more pronounced electronic change on the phenanthroline moiety. This has also been reported for electron deficient phenanthroline-based Ru^{II} complexes.[72,73] An electronic interaction was shown to to be possible in both positions, but more significant in the 4,7-position.[72]

Interestingly, among the novel series exclusively **Cu(CF$_3$)$_2$** owns a second reversible reduction at $E_{1/2}^{red}$= -2.22 V in the electrochemically accessible potential range of acetonitrile (Fig. 6). This is well in line with the discussion concerning the low-lying LUMO+2/+3 introduced by the $(CF_3)_2$ modification (*vide supra*, *e.g.* Fig. 4). **Cu(CF$_3$)$_2$** is therefore the only compound in this study that is twice reducible in acetonitrile (details *cf.* Fig. S7.5).

Further, as expected for these type of heteroleptic copper(I) complexes, they all show one irreversible oxidation, which is attributed to the literature-known oxidation of the Cu-P bond at around +0.9 V (ESI Figs. S7.1-4).[46,48,49,71,74]

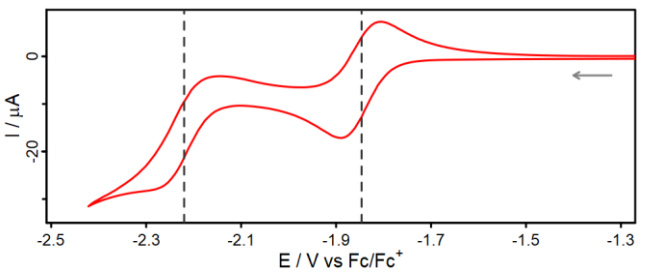

Fig. 6 Cyclic voltammogram of **Cu(CF$_3$)$_2$** displaying the two reduction events measured in inert acetonitrile ($E_{1/2}^{red}$ = -1.94 and -2.22 V *vs.* Fc/Fc$^+$). Among all the copper(I) complexes in the series a second reduction is exclusively present in **Cu(CF$_3$)$_2$**.

UV/vis Spectroscopy

The study of the absorption properties by UV/vis spectroscopy revealed a clear trend (see Fig. 7, Table 3): when moving from the most electron deficient **Cu(CF$_3$)$_2$** complex to the most electron donating **CuOMe**, the attenuation coefficients of the metal-to-ligand charge transfer (MLCT) band ε_{MLCT} steadily increase from $3.7 \cdot 10^3$ to $6.4 \cdot 10^3$ $M^{-1}cm^{-1}$ (by a factor of 1.7).

This observation is in contrast to our preceding study about substitution in 5,6-position, where electron withdrawing substituents seemed to increase the absorptivity.[48] In our current work, **CuOMe** represents the most strongly absorbing derivative ($6.4{\cdot}10^3$ $M^{-1}cm^{-1}$), while its 5,6-relative has been found to be the weakest absorbing species ($3.0{\cdot}10^3$ $M^{-1}cm^{-1}$).[48] The novel complexes exhibit a better absorptivity in most cases (*e.g.* $3.7{\cdot}10^3$ $M^{-1}cm^{-1}$ for the weakest absorbing 4,7-derivative *vs.* $4.0{\cdot}10^3$ $M^{-1}cm^{-1}$ for the strongest 5,6-derivative). In addition, the most electron deficient **Cu(CF$_3$)$_2$** complex absorbs at slightly red-shifted wavelength compared to its 5,6-counterpart (395 *vs.* 390 nm). Earlier studies on Ru^{II} phenanthroline complexes also discussed the tendency for the 4,7-position to have a greater effect on the absorptivity. However, these studies did not include electron donating substituents, and therefore could not confirm a decreasing absorptivity of electron rich groups in the 5,6-position.[72,73,75] In general, the MLCT absorption maxima of the novel complexes gradually shift to the blue as they adopt a more electron donating character (Table 3). This is also consistent with the analysis of the orbital energies discussed above (Table 2).

Table 3. Summary of the photophysical and electrochemical properties of the Cu(I) complexes in acetonitrile (MeCN) and dichloromethane (CH_2Cl_2) solution at room temperature under inert conditions. Reduction potentials $E_{1/2}^{red}$ and excited state reduction potentials $E^*_{1/2}{}^{red}$ are referenced *vs.* the ferrocene/ferricenium (Fc/Fc^+) couple. The zero-zero excitation energy $E_{0,0}$ has been calculated using the tangent-method as described in the ESI (see Chapter 10). The table also shows the results from catalytic singlet oxygen generation (singlet oxygen quantum yields ϕ_{1O2} were determined from integration of the emission signal of $^1O_2$).

Compound	λ_{abs} [nm] (ε [10^3 $M^{-1}cm^{-1}$])	λ_{em} [nm]^c (ϕ_{em} [%])^d		τ_{em} [µs]^e		$E_{1/2}^{red}$ [V]^{f,g}	$E_{0,0}$ [eV]	$E^*_{1/2}{}^{red}$ [V]^f	ϕ_{1O2} [%]
	MeCN	MeCN	CH_2Cl_2	MeCN	CH_2Cl_2	MeCN	MeCN	MeCN	CH_2Cl_2
Cu(CF$_3$)$_2$	395 (3.7)	613 (0.2)	598 (6)	0.04	1.5	-1.85; -2.22	2.43	0.58	37
CuCF$_3$	394 (4.22)	598 (0.4)	587 (19)	0.10	5.2	-1.93	2.47	0.54	47
CuF	387 (4.9)	583 (1.1)	574 (45)	0.25	12.5	-2.02	2.53	0.51	48
CuH	387 (5.2)^a	578 (1.35)^b	574 (53)	0.31^b	14.9	-2.04	2.53	0.49	46
CuOMe	382* (6.4)	573 (2.1)	568 (64)	0.63	21.0	-2.08	2.56	0.48	54

^{a} Taken from reference[62]. ^{b} Taken from reference[48]. ^{c} Excited at the respective absorption maximum. ^{d} Excited at 390 nm. ^{e} Excited at 355 nm. ^{f} Referenced against the ferrocene/ferricenium couple Fc/Fc^+. ^{g} Only reversible events are listed. * Due to a steady decrease of the absorption no maximum can be determine

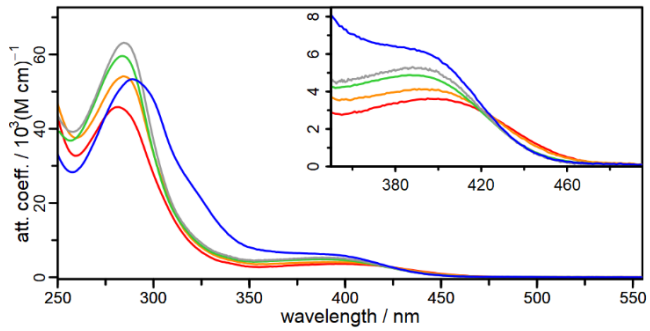

Fig. 7 UV/vis absorption spectra of the complexes **Cu(CF$_3$)$_2$**, **CuCF$_3$**, **CuF**, **CuH** and **CuOMe** (red, orange, green, grey and blue) in acetonitrile showing their respective attenuation coefficients relative to the absorbed wavelength. **Cu(CF$_3$)$_2$** absorbs most red-shifted (λ_{abs} = 395 nm). In the visible region (*i.e.* λ > 400 nm) **CuOMe** yet absorbs strongest.

The UV/vis spectroscopic results regarding the modification in 4,7-position can be summarized as follows: i) substitution generally induces a larger increase in absorptivity compared to the 5,6-position, ii) stronger electron donation increases the attenuation coefficients, and iii) a more pronounced red-shift of the absorption maxima compared to substitution in 5,6-position.[48] Thus, when considering the absorption properties alone, the 4,7-position seems superior over the 5,6-position for future substitution.

Steady-State and Time-resolved Emission Properties

Further studies included the investigation of the emission properties of the complexes in two different polar solvents. These were a coordinating (acetonitrile) and a non-coordinating solvent (dichloromethane), respectively,[76] which usually have a significant impact on the emission.[77,78] When the results from the steady-state emission are combined with the emission lifetime measurements, the general trend already observed in the discussions above remains.

Going from the most electron withdrawing **Cu(CF$_3$)$_2$** to the most electron donating **CuOMe** reveals a strong increase of all probed parameters of the emission process. In both solvents the maxima of the broad ^{3}MLCT emission in this series shift blue about 30-40 nm (Fig. 8), the emission quantum yields ϕ_{em} strongly increase by a factor of about 10 and the emission lifetimes steadily rise by a factor of about 15 (Table 3). These findings are in strong contrast to our previous study, where substitution in 5,6-position revealed the methoxy-substituted derivative as the compound with the lowest emission quantum yield ϕ_{em} (0.16%) and shortest emission lifetime τ_{em} (11 ns) in acetonitrile.[48] In fact, attaching any of the substituents in 5,6-position caused a strong decline of ϕ_{em} compared to the unsubstituted parent compound [Cu(2,9-dimethyl-1,10-phenanthroline)(xant)]$^+$.[48] In 4,7-position, a decrease of ϕ_{em} is also found for the two electron deficient CF_3 containing derivatives. The OMe functional group, however, drastically improves this parameter (factor ≈2.5).

It is again emphasised that in the present work, the most electron donating **CuOMe** has the most beneficial properties, *e.g.* high ϕ_{em} (2.1% and 64%) and strongly increased τ_{em} (0.63 µs and 21 µs) in acetonitrile and dichloromethane, respectively. The unsubstituted and well-studied benchmark

complex **CuH** shows significantly lower values concerning these parameters (ϕ_{em}=1.35 and 53%, τ_{em}=0.31 µs and 14.9 µs in acetonitrile and dichloromethane, respectively). The most electron deficient **Cu(CF$_3$)$_2$** possesses the smallest values (Table 3)(ϕ_{em} = 0.2 and 6%, τ_{em} = 0.04 µs and 1.5 µs in acetonitrile and dichloromethane, respectively). An additional transient absorption measurement did not reveal any significant discrepancy to the emission lifetime of **Cu(CF$_3$)$_2$** proving that the longest-lived state is the emissive state (data not shown). Attaching electron deficient substituents in 4,7-position also strongly affects the emission wavelength (*ca.* 50 nm for $(CF_3)_2$ *vs.* the unsubstituted parent complex). The effect is, however, much smaller for the 5,6-position (*ca.* 1 nm for $(CF_3)_2$).[48] In related Ru complexes, an analogues behaviour has been found for electron deficient groups when comparing both positions.[72,73,75]

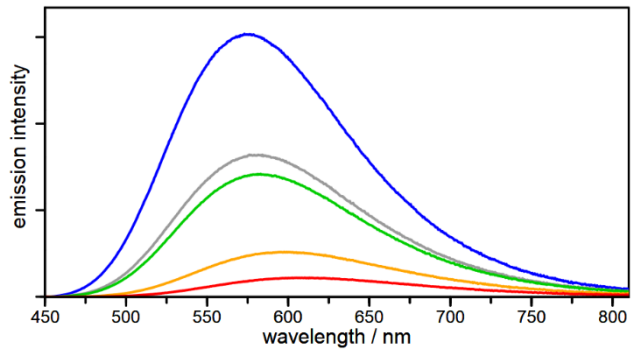

Fig. 8 Corrected emission spectra of **Cu(CF$_3$)$_2$**, **CuCF$_3$**, **CuF**, **CuH** and **CuOMe** (red, orange, green, grey and blue, respectively) measured in inert acetonitrile excited at the respective absorption maxima λ_{abs}. The optical densities were adjusted to around 0.1 at λ_{abs} to ensure comparability of the emission intensities.

Subsequently, the radiative (k_r) and non-radiative (k_{nr}) rate constants were estimated (for details see ESI Chapter 9) from τ_{em} and ϕ_{em}.[79] The k_r values of the complexes presented here are quite similar when comparing acetonitrile and dichloromethane. Further, the k_r values decrease only slightly within the series (*e.g.* from $4.0\cdot10^4$ to $3.0\cdot10^4$ s^{-1} with increasing electron donating character). In contrast, k_{nr} decreases strongly within the series in both solvents ($6.3\cdot10^5$ to $1.7\cdot10^4$ s^{-1} in dichloromethane, $2.5\cdot10^7$ to $1.6\cdot10^6$ s^{-1} in acetonitrile, ESI Table S9.1). It can be concluded that the solvent and the choice of the functional group have little effect on k_r, while k_{nr} is strongly influenced by the functional group. This is likely due to the decreased excited state energy in the electron deficient derivatives, where according to the energy gap law, non-radiative transitions are more likely to occur as a result of increased overlap of vibrational states (leading to faster internal conversion).[77,79] For these reasons **CuOMe** has the most favorable characteristics.

In general, the k_{nr} constants are much greater in acetonitrile compared to dichloromethane. For example, the k_{nr} of the electron rich **CuOMe** is about 100 times larger ($1.6\cdot10^6$ *vs.* $0.017\cdot10^6$ s^{-1}). This is due to literature known quenching of the excited state by coordinating acetonitrile molecules (exciplex quenching).[80,81]

Looking at the corresponding literature-known[48] derivatives with the same substituents, but in 5,6-position, the k_{nr} values are in the same range compared to the 4,7-series (ESI Table S9.1). This is not the case for the 5,6-substituted OMe derivative, which has not the lowest, but by far the highest k_{nr} ($90.8\cdot10^6$ s^{-1}). Interestingly, also k_r decreases significantly with increasing donating character, which is in contrast to their 4,7-substituted counterparts. Again, with the exception of the OMe derivative, as also its k_r value is the highest among all derivatives (5,6- and 4,7-position, *cf.* ESI Table S9.1).

Excited State Reduction Potentials $E^*_{1/2}{}^{red}$

To enable a more well-founded discussion on the catalytic performance and perspective applications of the copper(I) complexes, the corresponding exited state reduction potentials $E^*_{1/2}{}^{red}$ were estimated from the experimental reduction potentials $E_{1/2}{}^{red}$ and the zero-zero excitation energy $E_{0,0}$ using the Rehm-Weller equation (see ESI Chapter 10 for details).[82] Although the exact determination of the excited state potentials is challenging, a comparison among the derivatives is nevertheless useful, especially since the maximum difference between the compounds can be up to 100 mV, which is of great importance for the discussion (methodological details are given in Chapter 10 in the ESI).

In general, the $E^*_{1/2}{}^{red}$ of the heteroleptic complexes (Table 3) are significantly higher in comparison to those of typical homoleptic copper(I) complexes, which are known to be rather poor photo oxidants ($E^*_{1/2}{}^{red}$ typically below 0 V *vs.* Fc/Fc^+).[23,34,83,84]

Interestingly, **Cu(CF$_3$)$_2$** reveals the highest $E^*_{1/2}{}^{red}$ (0.58 V for **Cu(CF$_3$)$_2$** *vs.* 0.48 V for **CuOMe**) within this series. Therefore, beside lacking a comparably long-lived excited state and a high quantum yield, **Cu(CF$_3$)$_2$** represents the strongest excited state oxidant among the copper(I) complexes presented herein. Compared to the well-known **CuH** ($E^*_{1/2}{}^{red}$ = 0.49 V) the excited state reduction potential is increased by 90 mV. **Cu(CF$_3$)$_2$** can therefore be highlighted as an interesting candidate for further catalytic studies – as long as efficient quenching processes are possible.

Catalytic Oxygenation with Singlet Oxygen

Singlet oxygen ($^1O_2$) is the energetically rich form of molecular oxygen and can be applied in the photodynamic therapy (PDT) of cancer but also is often used in in organic chemistry as an effective and selective oxidizing agent.[52-54] Typically, $^1O_2$ is generated via energy transfer from the excited state of a photosensitizer to triplet oxygen ($^3O_2$). $^1O_2$ has a characteristic emission peak (phosphorescence) in the near-infrared around 1270 nm, corresponding to the energy difference of 94.3 kJ/mol between $^1O_2$ and $^3O_2$.[52,53] Hence, the catalytic generation of $^1O_2$ can be accessed by measuring the NIR emission of $^1O_2$ in reference to phenalenone as an universal standard.[85-89] From previous studies on related copper compounds it is known, that the singlet oxygen quantum yield ϕ_{1O2} in acetonitrile is usually comparatively low,[45,46] which is

also the case here. The ϕ_{1O2} were therefore determined in dichloromethane instead (see Table 3). As expected, the ϕ_{1O2} increases with increasing electron donation (*e.g.* from 37% in **Cu(CF$_3$)$_2$** to 54% in **CuOMe**). Although the emission quantum yield and the emission lifetime of **Cu(CF$_3$)$_2$** are clearly decreased compared to **CuOMe**, the ϕ_{1O2} of **Cu(CF$_3$)$_2$** is still relatively high (*i.e.* 70% of that of **CuOMe**). Note, that the absence of any sacrificial electron donor and the control absorption spectra of **CuOMe** and **Cu(CF$_3$)$_2$** before and after singlet oxygen generation (ESI Fig. S11.20) render the formation of reduced forms of oxygen such as superoxide ($O_2^{\bullet-}$) unlikely. The fact that the ϕ_{1O2} of **Cu(CF$_3$)$_2$** is comparably high may already indicate that its activity should not be underestimated based on its low ϕ_{em} and τ_{em}.

In order to evaluate their applicability, the catalytic oxygenation of 2,5-diphenylfuran (DPF) to *cis*-dibenzoylethylene (DBE) was chosen as a model reaction (see Fig. 9).[52,55-57] Importantly, neither DPF nor DBE absorbs above 380 nm, precluding a competitive light absorption with the PS when using visible light exclusively (for details on the catalytic setup, please see ESI Chapter 11 and Fig. S11.18). The reactions of the respective CuPS with DPF were continuously followed by *in situ* UV-vis spectroscopy. The consumption of DPF and formation of DBE were analysed at their characteristic bands at 324 nm (decreasing DPF) and 255 nm (increasing DBE) over a period of at least 90 min (*e.g.* Fig. 9 and ESI Chapter 11). The overall yields were calculated using the attenuation coefficient of DBE (ε = 18.1·10^3 M^{-1}cm^{-1}).[90,91] Additional experiments confirmed the stability of the photosensitizers and DPF under the chosen conditions (ESI Fig. S11.14-16), and the necessity of light and the PSs themselves to achieve conversion (ESI Fig. S.11.17).

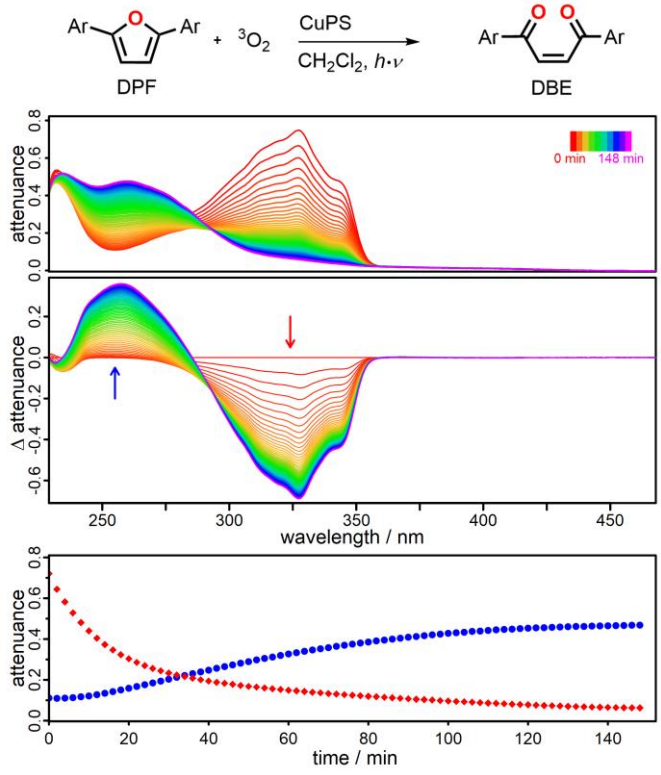

Fig. 9. Top: Spectra evolution of the reaction of 2,5-diphenylfuran (DPF, c = 2·10^{-5} M) to *cis*-dibenzoylethylene (DBE) sensitized by **CuOMe** (DPF:CuOMe = 10:1) in aerated dichloromethane at room temperature followed until completion (for all other spectra see ESI Chapter 11). **Center:** Difference spectra of the recorded spectra shown above (arrows indicate the direction and the selected wavelengths 255 nm, blue, and 324 nm, red). **Bottom:** Kinetic traces of the two selected wavelengths 324 nm (absorption maximum DPF, red arrow center and red dots bottom) and 255 nm (absorption maximum DBE, blue arrow center and blue dots bottom).

As a result, the formation of DBE correlates well with the respective singlet oxygen quantum yields ϕ_{1O2} and increases steadily within the series (ESI Table S11.2). After 90 min, 83% of DBE was produced by **CuOMe**, while **Cu(CF$_3$)$_2$** achieved 52%. **CuOMe** completed the reaction after around 2 hours (>99% DBE, Fig. 9).

More detailed kinetic analysis showed that the consumption of DPF follows a first order kinetic during the first 15 minutes and is similar for all complexes (within 10% error, ESI Table S11.3). Therefore, the early kinetics do not significantly depend on the chosen CuPS, likely due to the high concentration of $^3O_2$.[103] The formation of DBE starts with a delay of about 5-10 minutes and then increases sharply, while an assumed first order kinetics does not seem to be valid. This is reasonable due to the literature known formation of an intermediate, from which the DBE forms subsequently.[55,92] Nevertheless, applying the rate law yields two rate constants which are within the error largest for **CuOMe** and smallest for **Cu(CF$_3$)$_2$**. This confirms, that the most electron rich derivative induces the fastest formation of the desired product under the chosen conditions. In fact, the singlet oxygen quantum yields directly correlate with the product formation. This means that when comparing the rate constants of DBE formation, the same factor of 1.5 is found as when comparing the ϕ_{1O2} of **CuOMe** and **Cu(CF3)2**.

Photoinduced reductive dehalogenation

To further explore the capability of this new series of complexes, their reactivity in the context of a basic organic transformation were examined. In this respect, the photocatalytic reductive dehalogenation of aryl halides represents a relevant benchmark reaction, which has been investigated in many past contributions.[93-95] Briefly, the reaction involves the cleavage of the carbon-halogen bond by reducing aryl halides Ar-X into the radical Ar• and the halide X$^-$, followed by protonation of Ar• leading to Ar-H (see Scheme 1). In the case of copper(I) complexes, such strong reductive power is achieved when the excited state of the latter is reductively quenched by a sacrificial donor, affording the reduced copper(I) complex in its ground state. As shown in Table 3, all complexes indeed feature a significantly negative reduction potential (between -1.85 and -2.08 V *vs.* Fc$^+$/Fc couple).

Our first goal was to determine and to compare the photocatalytic activity of all complexes under the same conditions. For this purpose, 2-bromoacetanilide **1-Br** was selected as Ar-X substrate and BI$_1$H as sacrificial donor (BI$_1$H = 5-methoxy-2-(4-methoxyphenyl)-1,3-dimethyl-2,3-dihydro-1H-benzo[d]imidazole, Scheme 1). BI$_1$H was chosen because it has

a substantially lower oxidation potential compared to the more traditional triethylamine (ca. 0.35 V and 0.7 V *vs.* SCE, respectively) and is therefore expected to increase the driving force of the reductive quenching step.[96-98] All reactants, namely **1-Br**, BI_1H and the copper(I) complex (1 mol%) were dissolved in acetonitrile and degassed, before the mixture was irradiated with light (blue LED, 450 nm) for a maximum of 3 hours under vigorous stirring (Fig. S12.1).

Table 4. Results of the photochemical dehalogenation experiments. Conditions: substrate = 0.1 mmol, catalyst = 1 mol% in inert acetonitrile unless otherwise specified, blue LED (for further details see ESI chapter 10). TON stands for turnover number and TOF for turnover frequency.

1-Br **1-H**

Entry	Catalyst	Donor	Time [h]	Conversion [%] (Yield [%])[b]	TON	TOF [h^{-1}]	Conversion [%] at 5 and 15 min
1	**CuOMe**	none	3	0	-	-	n.d.[d]
2	none	BI_1H	3	0	-	-	n.d.
3	**CuOMe**[a]	BI_1H	3	0	-	-	n.d.
4	**CuOMe**[c]	BI_1H	1	99 (89)	18	18	n.d.
5	**CuOMe**	BI_1H	3	97 ± 2 (87)	87 ± 3	29 ± 1	11, 32
6	**CuH**	BI_1H	3	99 ± 0.5 (87)	87 ± 3	29 ± 1	16, 44
7	**$Cu(CF_3)_2$**	BI_1H	3	97 ± 2 (92)	92 ± 2	30 ± 1	39, 61
8	**$CuCF_3$**	BI_1H	3	97 ± 3 (91)	91 ± 2	30 ± 1	11, 35
9	**CuF**	BI_1H	3	97 ± 2 (88)	88 ± 3	29 ± 1	16, 38

[a] No light, [b] GC yield with hexadecane as internal standard, [c] **CuOMe** = 5 mol%, [d] n.d.: not determined

All results are summarized in Table 4, while the time evolution of the conversion can be found in Fig. S12.2.

An initial catalyst loading of 5 mol% was used, resulting in a spectacularly efficient and fast conversion (89% yield within only 1 hour) of **1-Br** to **1-H** (Table 4, entry 4). This encouraged us to significantly decrease the loading to 1 mol%. Under these conditions, all complexes proved to be excellent photocatalysts, converting **1-Br** into **1-H** very efficiently (conversions of at least 97% and yields between 87 and 92%) and still very quickly as the reactions are completed after 3 hours of irradiation (Table 4, entries 5-9). For comparison, 24 hours are required for similar previously published reactions.[16,93] Blank experiments confirmed the necessity to gather all partners in order to observe any reaction and that the reaction is light-driven (Table 4, entries 1-3). Stern-Volmer experiments verified that the reaction proceeds through reductive quenching and not by oxidative quenching. This means that the emission lifetimes of the photo-excited complexes steadily decrease upon addition of BI_1H, whereas they are unaffected by the presence of **1-Br** (ESI Figs. S12.3 and S12.4).

The photocatalytic results do not allow a clear comparison between the differently substituted copper(I) complexes, because they all work so well. Nevertheless, when focusing on the first minutes of catalysis, slight differences can be found (Fig. S12.5). The fastest dehalogenation reaction is observed when **$Cu(CF_3)_2$** is used as photocatalyst, closely followed by **CuH** and more sluggish reactions are obtained with **CuF**, **$CuCF_3$** and **CuOMe**.

The absorbances of the solutions in the irradiation zone (ca. 460 nm, Figure S12.6) are weak for all complexes and unlikely to account for the observed differences, especially given the wavelength width of the LED beam.

From the thermodynamic point of view, **$[Cu(CF_3)_2]^-$** and **$[CuOMe]^-$** are respectively the least and the most reductive complexes of the series, and yet photocatalysis with **$Cu(CF_3)_2$** and with **CuOMe** are respectively the fastest and the most sluggish. This demonstrates that the reduction of **1-Br** (E_{red} = -2.65 V *vs.* Fc^+/Fc, Fig. S12.7 and comments) is probably not a kinetically determining step. The reductive quenching step would therefore be kinetically determining, namely when the photo-excited complex reacts with the sacrificial donor **BI_1H**.

This is consistent with the reductive quenching constant k_{RQ} obtained for the quenching of excited **$Cu(CF_3)_2$*** by BI_1H (Stern-Volmer plots, $k_{RQ} = 7.6 \cdot 10^9$ $M^{-1}s^{-1}$), which is the highest among the series. This is however counter-balanced by the short excited state lifetime of **$Cu(CF_3)_2$*** leading to the smallest K_{SV} value of the series (Table S12.1). Besides, **CuOMe*** exhibits the highest K_{SV}, and the second best k_{RQ}, and yet the dehalogenation reaction photocatalysed by **CuOMe** is among the most sluggish ones.

Table 5. Substrate scope of the photochemical dehalogenation experiments. Conditions: **CuOMe** = 1 mol% in 3 mL of acetonitrile (MeCN), 0.2 mmol BI_1H and 0.1 mmol R-X.

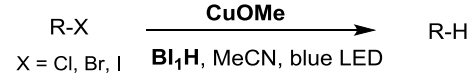

Entry	Substrate	Time	Conversion [%] (Yield [%])[a]	TON	TOF [h^{-1}]
1	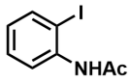	1 h	99 ± 0.5 (96)	96	96
2	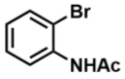	3 h	97 ± 2 (87)	87	29
3	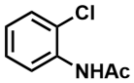	24 h	4.3 ± 0.5 (n.d.)[b]	n.d.	n.d.
4	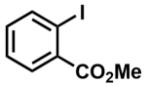	2 min	99 ± 0.5 (97)	97	2939
5	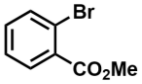	5 min	99 ± 0.5 (98)	98	1180
6	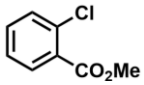	30 min	99 ± 0.5 (95)	95	190
7		5 h	99 ± 0.5 (80)	80	16
8	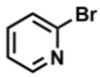	24 h	99 ± 0.5 (96)	96	4
9		24 h	7 ± 2 (n.d.)	n.d.	n.d.

[a] GC yield with hexadecane as internal standard, [b] n.d.: not determined

This highlights the fact that the electron transfer from the excited copper(I) complexes to BI_1H may occur with different efficiencies, but that does not affect the overall kinetics of the dehalogenation reaction. Incidentally, those considerations once more underline that the excited state reactivity of copper complexes is notoriously difficult to anticipate.[99]

This result can tentatively be rationalized by considering that the initial photo-induced electron transfer occurs within a cage [complex-BI_1H].[100-102] After photo-induced electron transfer, back charge recombination can occur very efficiently within the cage, if the reduced complex and BI_1H^+ do not diffuse away from each other fast enough. This is described as cage escape yield, and sensitizers with mixed singlet and triplet excited state character are known to have lower cage escape yields.[100] Thus, the discrepancies observed here could be due to a better cage escape yield for **Cu(CF$_3$)$_2$** and **CuH** compared to **CuOMe**, **CuF** and **CuCF$_3$** Nevertheless, the four new complexes are all excellent photocatalysts in the framework of a dehalogenation reaction. Incidentally, our results demonstrate that even though **Cu(CF$_3$)$_2$** is endowed with a short excited state lifetime (40 ns, the shortest lifetime of the series), this does not prevent it from outperforming the other photocatalysts, including the benchmark **CuH**.[103]

We next explored the scope of this reaction with other substrates (Scheme 1 and Table 5). For this purpose, we focused on the most reductive complex **CuOMe**, because only the strongest reductants can react with challenging substrates, such as aryl chlorides. As can be seen in Table 5, all iodinated and brominated molecules were reduced, regardless of the nature of the substrate. The efficiency of the reaction is particularly striking, with maximum turnover frequencies (TOF) of about 2900 and 1200 for aryl iodides and aryl bromides, respectively (Table 5, entries 4 and 5). In contrast, aryl chlorides are more difficult to reduce and more challenging substrates because the C-Cl bond is harder to activate (Table 5, entries 2 and 6).[13,23] However, 2-chloromethylbenzoate, the electron poorer aryl chloride, was successfully dechlorinated in only 30 min, with a respectable turnover number (TON) and TOF of 95 and 190 h^{-1}, respectively. This is a very encouraging result for future prospects in the functionalization and late stage modification of aryl chlorides.

The fluorinated substrate 2-fuorobenzoate was also subjected to catalysis, but remained unchanged even after 24 h. This marks an important limitation of the studied complexes, which describes the demand for continued efforts to tune their excited state properties.

Finally, we also aimed to demonstrate the possibility to scale up this reaction. Therefore, the benchmark dehalogenation reaction of **1-Br** was performed using 1 mol% of **CuOMe** with 1 mmol of substrate instead of 0.1 mmol. A very satisfying yield of 84% was obtained, although a longer reaction time was required (24 hours) leading to a TOF of 3.5 h^{-1}. A further decrease of the catalyst loading to 0.1 mol% led to a respectable yield of 54% after 48 hours of irradiation, affording a TON of 540 and TOF of 11 h^{-1}. This demonstrates the relevance to use copper(I) complexes as photocatalysts in modern photochemistry.

Conclusions

Copper(I)-based complexes can be successfully used as photosensitizers and photocatalysts, although the underlying structure-property relationships are not yet fully understood. Therefore, this study examined the effect of different electron withdrawing and donating groups at the 4,7-position of 1,10-pheanthroline in a new series of heteroleptic diimine-diphosphine copper(I) complexes. Apart from the electronic impact also major differences to the 5,6-position were uncovered on the basis of a previous study.[48]

Indeed, opposite trends were found concerning the absorption properties of the resulting complexes. While electron donating substituents in the 4,7-position increase the absorptivity, the same substituents in 5,6-position cause a reduced absorptivity compared to the unsubstituted complex. Similar observations were made for the emission properties. Emission lifetimes and quantum yields increase steadily with rising electron donating character, as also described in the literature.[47,49] Therefore, the **CuOMe** complex containing two methoxy substituents exhibits the highest values (*e.g.* τ_{em} = 630 ns and ϕ_{em} = 2.1% in MeCN) among this series. This is in strong contrast to the related complex with methoxy groups in the 5,6-position, where the same functional group gave the least favorable properties (*e.g.* τ_{em} = 11 ns and ϕ_{em} = 0.16% in MeCN).[48] Besides the methoxy groups, especially bistrifluoromethyl substituents and the resulting **Cu(CF$_3$)$_2$** complex provide some unique properties. **Cu(CF$_3$)$_2$** is not only the strongest excited state oxidant ($E^*_{1/2}{}^{red}$ = 0.58 V), but also the exclusive complex that can be reduced twice. The accompanying DFT calculations indicated that **Cu(CF$_3$)$_2$** has especially low-lying, unoccupied orbitals localized on the substituents.

Most importantly, these photoactive Cu(I) complexes succeeded in two different photocatalytic applications, *i.e.* in the generation of reactive singlet oxygen and the subsequent photooxygenation of DPF, as well as in the dehalogenation of aryl halides. All complexes efficiently sensitize triplet to singlet oxygen with a maximum singlet oxygen quantum yield ϕ_{1O2} of 54% for the **CuOMe** derivative, which also causes the fastest conversion of DPF to DBE. This is consistent with the photophysical properties of **CuOMe**, as ϕ_{1O2} increases steadily with increasing ϕ_{em} and τ_{em}.

A breakthrough for such copper(I) complexes was achieved in the reductive dehalogenation of various aryl halides, including the challenging 2-chloropyridine. It was demonstrated that the suitable redox potentials of these complexes in the ground and excited states enable efficient dehalogenation of different substrates. For instance, methyl 2-bromo- and 2-iodobenzoate are both converted to methyl benzoate in high yields of 98% and extremely fast, with a maximum turnover frequency of 1180 and 2939 h^{-1}, respectively. Some preliminary experiments evidenced that the reaction can be scaled up and the catalyst loading reduced to only 0.1 mol%. This makes these heteroleptic copper(I) complexes a new benchmark for noble metal-free systems.

The striking differences between substitution at the 5,6 and 4,7 positions as well as other photocatalytic applications, such as the light-driven reduction of CO_2, are the subject of ongoing investigations in our laboratories.

Author Contributions

FD envisioned the project and synthesised, purified and characterized the ligands and respective complexes. FD performed the electrochemical and photophysical measurements as well as singlet oxygen generation studies and DFT calculations. YP and CQ designed and performed the catalytic dehalogenation experiments. FD, MK, YP, CQ and ST analysed and discussed the data. MK, YP, CQ and ST guided the research and revised the manuscript. All authors approved the final version of the publication.

Conflicts of interest

The authors declare no competing financial interests.

Acknowledgements

This work was supported by the Deutsche Forschungs-gemeinschaft (DFG) within the Priority Program SPP 2102 “Light-controlled reactivity of metal complexes” (TS 330/4-1 and KA 4671/2-1). We thank the RWTH Aachen Compute Cluster (Project No. 4706) for the provision of computing time. We are also thankful to the group of Prof. Christoph Jacob (TU Braunschweig) for access to their compute cluster. Great acknowledgment is attributed to Lars E. Burmeister (TU Braunschweig) for his support concerning the spectroscopic measurements.

Notes and references

‡ The CCDC reference numbers for **CuOMe** (2237580) and **Int** (2237581) contain the supplementary crystallographic data for this paper. These data can be obtained free of charge via www.ccdc.cam.ac.uk/data_request/cif or by emailing data_request@ccdc.cam.ac.uk or by contacting The Cambridge Crystallographic Data Centre, 12 Union Road, Cambridge CB2 1EZ, UK.

1 R. C. Evans, P. Douglas and C. J. Winscom, *Coord. Chem. Rev.,* 2006, **250,** 2093-2126.
2 C. Borek, K. Hanson, P. I. Djurovich, M. E. Thompson, K. Aznavour, R. Bau, Y. Sun, S. R. Forrest, J. Brooks, L. Michalski and J. Brown, *Angew. Chem. Int. Ed.,* 2007, **46,** 1109-1112.
3 J. G. Williams, S. Develay, D. L. Rochester and L. Murphy, *Coord. Chem. Rev.,* 2008, **252,** 2596-2611.
4 C. Bizzarri, E. Spuling, D. M. Knoll, D. Volz and S. Bräse, *Coord. Chem. Rev.*, 2018, **373**, 49-82.
5 R. D. Costa, E. Ortí, H. J. Bolink, F. Monti, G. Accorsi and N. Armaroli, *Angew. Chem. Int. Ed.,* 2012, **51,** 8178-8211.
6 S. Keller, A. Prescimone, M.-G. La Placa, J. M. Junquera-Hernández, H. J. Bolink, E. C. Constable, M. Sessolo, E. Ortí and C. E. Housecroft, *RSC Adv.,* 2020, **10,** 22631-22644.
7 C. E. Housecroft and E. C. Constable, *J. Mater. Chem. C,* 2022, **10,** 4456-4482.
8 M. Grätzel, *Inorg. Chem.,* 2005, **44,** 6841-6851.
9 A. Hagfeldt, G. Boschloo, L. Sun, L. Kloo and H. Pettersson, *Chem. Rev.,* 2010, **110,** 6595-6663.

10 F. Odobel, Y. Pellegrin, E. A. Gibson, A. Hagfeldt, A. L. Smeigh and L. Hammarström, *Coord. Chem. Rev.,* 2012, **256,** 2414-2423.
11 D. Devadiga, M. Selvakumar, P. Shetty and M. S. Santosh, *J. Power Sources,* 2021, **493,** 229698.
12 K. Zeitler, *Angew. Chem. Int. Ed.,* 2009, **48,** 9785-9789.
13 C. K. Prier, D. A. Rankic and D. W. C. MacMillan, *Chem. Rev.,* 2013, **113,** 5322-5363.
14 D. M. Schultz and T. P. Yoon, *Science,* 2014, **343,** 1239176.
15 L. Marzo, S. K. Pagire, O. Reiser and B. König, *Angew. Chem. Int. Ed.,* 2018, **57,** 10034-10072.
16 J.-H. Shon, D. Kim, M. D. Rathnayake, S. Sittel, J. Weaver and T. S. Teets, *Chem. Sci.,* 2021, **12,** 4069-4078.
17 B. M. Hockin, C. Li, N. Robertson and E. Zysman-Colman, *Catal. Sci. Technol.,* 2019, **9,** 889-915.
18 H. Yuan, B. Cheng, J. Lei, L. Jiang and Z. Han, *Nat. Commun.,* 2021, **12,** 1835.
19 H. Kim and C. Lee, *Angew. Chem. Int. Ed.,* 2012, **51,** 12303-12306.
20 E. D. Nacsa and D. W. C. MacMillan, *J. Am. Chem. Soc.,* 2018, **140,** 3322-3330.
21 R. C. McAtee, E. J. McClain and C. R. J. Stephenson, *Trends Chem.,* 2019, **1,** 111-125.
22 J. D. Nguyen, E. M. D'Amato, J. M. R. Narayanam and C. R. J. Stephenson, *Nat. Chem.,* 2012, **4,** 854-859.
23 L. Gimeno, C. Queffélec, K. Mall Haidaraly, E. Blart and Y. Pellegrin, *Catal. Sci. Technol.,* 2021, **11,** 6041-6047.
24 S. Styring, *Faraday Discuss.,* 2012, **155,** 357-376.
25 S. Berardi, S. Drouet, L. Francàs, C. Gimbert-Suriñach, M. Guttentag, C. Richmond, T. Stoll and A. Llobet, *Chem. Soc. Rev.,* 2014, **43,** 7501-7519.
26 Y.-J. Yuan, Z.-T. Yu, D.-Q. Chen and Z.-G. Zou, *Chem. Soc. Rev.,* 2017, **46,** 603-631.
27 K. E. Dalle, J. Warnan, J. J. Leung, B. Reuillard, I. S. Karmel and E. Reisner, *Chem. Rev.,* 2019, **119,** 2752-2875.
28 Z. Chen, H. Junge and M. Beller, *Front. Chem.,* 2022, **16,** 697-699.
29 H. B. Gray, *Nat. Chem.,* 2009, **1,** 7.
30 P. Du and R. Eisenberg, *Energy Environ. Sci.,* 2012, **5,** 6012.
31 Y. Zhang, M. Schulz, M. Wächtler, M. Karnahl and B. Dietzek, *Coord. Chem. Rev.,* 2018, **356,** 127-146.
32 C. B. Larsen and O. S. Wenger, *Chem. Eur. J.,* 2018, **24,** 2039-2058.
33 C. Förster and K. Heinze, *Chem. Soc. Rev.,* 2020, **49,** 1057-1070.
34 N. Armaroli, *Chem. Soc. Rev.,* 2001, **30,** 113-124.
35 M. Sandroni, Y. Pellegrin and F. Odobel, *C.R. Chim.,* 2016, **19,** 79-93.
36 M. Zhong, X. Pannecoucke, P. Jubault and T. Poisson, *Beilstein J. Org. Chem.,* 2020, **16,** 451-481.
37 C. Sandoval-Pauker, G. Molina-Aguirre and B. Pinter, *Polyhedron,* 2021, **199,** 115105.
38 J. Beaudelot, S. Oger, S. Peruško, T.-A. Phan, T. Teunens, C. Moucheron and G. Evano, *Chem. Rev.,* 2022, **122,** 16365-16609.
39 A. I. B. Romo, M. P. dos Reis, O. R. Nascimento, P. V. Bernhardt, J. Rodríguez-López and I. C. N. Diógenes, *Coord. Chem. Rev.,* 2023, **477,** 214943.
40 P. A. Forero Cortés, M. Marx, M. Trose and M. Beller, *Chem. Catal.,* 2021, **1,** 298-338.
41 M.-A. Schmid, M. Rentschler, W. Frey, S. Tschierlei and M. Karnahl, *Inorganics,* 2018, **6,** 134.
42 R. Giereth, I. Reim, W. Frey, H. Junge, S. Tschierlei and M. Karnahl, *Sustainable Energy Fuels,* 2019, **3,** 692-700.
43 S. Saeedi, C. Xue, B. J. McCullough, S. E. Roe, B. J. Neyhouse and T. A. White, *ACS Appl. Energy Mater.,* 2019, **2,** 131-143.
44 N. Arnosti, M. Meyer, A. Prescimone, E. Constable and C. Housecroft, *Crystals,* 2021, **11,** 185.
45 M. A. Argüello Cordero, P. J. Boden, M. Rentschler, P. Di Martino-Fumo, W. Frey, Y. Yang, M. Gerhards, M. Karnahl, S. Lochbrunner and S. Tschierlei, *Inorg. Chem.,* 2022, **61,** 214-226.
46 Y. Yang, F. Doettinger, C. Kleeberg, W. Frey, M. Karnahl and S. Tschierlei, *Front. Chem.,* 2022, **10,** 936863.
47 J. Kim, D. R. Whang and S. Y. Park, *ChemSusChem,* 2017, **10,** 1883-1886.
48 F. Doettinger, Y. Yang, M.-A. Schmid, W. Frey, M. Karnahl and S. Tschierlei, *Inorg. Chem.,* 2021, **60,** 5391-5401.
49 H. Takeda, Y. Monma, H. Sugiyama, H. Uekusa and O. Ishitani, *Front. Chem.,* 2019, **7,** 418.
50 H. Takeda, Y. Monma and O. Ishitani, *ACS Catal.,* 2021, **11,** 11973-11984.
51 C. Hansch, A. Leo and R. W. Taft, *Chem. Rev.,* 1991, **91,** 165-195.
52 A. Greer, *Acc. Chem. Res.,* 2006, **39,** 797-804.
53 P. R. Ogilby, *Chem. Soc. Rev.,* 2010, **39,** 3181-3209.
54 X. Li, S. Lee and J. Yoon, *Chem. Soc. Rev.,* 2018, **47,** 1174-1188.
55 Y. Usui, H. Koike and Y. Kurimura, Bull., *Chem. Soc. Jpn*., 1987, **60**, 3373-3378.
56 J. Al-Nu'airat, I. Oluwoye, N. Zeinali, M. Altarawneh and B. Z. Dlugogorski, *Chem. Rec.*, 2021, **21**, 315-342.
57 T. Montagnon, M. Tofi and G. Vassilikogiannakis, *Acc. Chem. Res.* 2008, **41**, 1001-1011.
58 E. H. Discekici, N. J. Treat, S. O. Poelma, K. M. Mattson, Z. M. Hudson, Y. Luo, C. J. Hawker and J. Read de Alaniz, *Chem. Commun.,* 2015, **51,** 11705-11708.
59 Q. Wang, M. Poznik, M. Li, P. J. Walsh and J. J. Chruma, *Adv. Synth. Catal.,* 2018, **360,** 2854-2868.
60 F. Glaser, C. B. Larsen, C. Kerzig and O. S. Wenger, *Photochem. Photobiol. Sci.,* 2020, **19,** 1035-1041.
61 T. Kinzel, Y. Zhang and S. L. Buchwald, *J. Am. Chem. Soc.,* 2010, **132,** 14073-14075.
62 J. E. Nycz, J. Wantulok, R. Sokolova, L. Pajchel, M. Stankevič, M. Szala, J. G. Malecki and D. Swoboda, *Molecules,* 2019, **24,** 4102.
63 B. Sahoo, P. Bellotti, F. Juliá-Hernández, Q.-Y. Meng, S. Crespi, B. König and R. Martin, *Chem. Eur. J.,* 2019, **25,** 9001-9005.
64 Y. Zhao, M. G. Schwab, A. Kiersnowski, W. Pisula, M. Baumgarten, L. Chen, K. Müllen and C. Li, *J. Mater. Chem. C,* 2016, **4,** 4640-4646.
65 Y. Zhang, M. Heberle, M. Wächtler, M. Karnahl and B. Dietzek, *RSC Adv.,* 2016, **6,** 105801-105805.
66 M. Heberle, S. Tschierlei, N. Rockstroh, M. Ringenberg, W. Frey, H. Junge, M. Beller, S. Lochbrunner and M. Karnahl, *Chem. Eur. J.,* 2017, **23,** 312-319.
67 E. Mejía, S.-P. Luo, M. Karnahl, A. Friedrich, S. Tschierlei, A.-E. Surkus, H. Junge, S. Gladiali, S. Lochbrunner and M. Beller, *Chem. Eur. J.,* 2013, **19,** 15972-15978.
68 A. Kaeser, M. Mohankumar, J. Mohanraj, F. Monti, M. Holler, J.-J. Cid, O. Moudam, I. Nierengarten, L. Karmazin-Brelot, C. Duhayon, B. Delavaux-Nicot, N. Armaroli and J.-F. Nierengarten, *Inorg. Chem.,* 2013, **52,** 12140-12151.
69 K. E. Riley, B. T. Op't Holt and K. M. Merz, *J. Chem. Theory Comput.,* 2007, **3,** 407-433.
70 J. Aragó, P. M. Viruela, E. Ortí, R. Malavé Osuna, V. Hernández, J. T. López Navarrete, C. R. Swartz and J. E. Anthony, *Theor. Chem. Acc.,* 2011, **128,** 521-530.
71 M. Rentschler, P. J. Boden, M. A. Argüello Cordero, S. T. Steiger, M.-A. Schmid, Y. Yang, G. Niedner-Schatteburg, M. Karnahl, S. Lochbrunner and S. Tschierlei, *Inorg. Chem.,* 2022, **61,** 12249-12261.
72 E. Sakuda, Y. Ando, A. Ito and N. Kitamura, *Inorg. Chem.*, 2011, **50**, 1603-1613.

73 G. V. Morozkov, A. S. Abel, M. A. Filatov, S. E. Nefedov, V. A. Roznyatovsky, A. V. Cheprakov, A. Yu. Mitrofanov, I. S. Ziankou, A. D. Averin, I. P. Beletskaya, J. Michalak, C. Bucher, L. Bonneviot and A. Bessmertnykh-Lemeune, *Dalton Trans.*, 2022, **51**, 13612-13630.

74 S. Fischer, D. Hollmann, S. Tschierlei, M. Karnahl, N. Rockstroh, E. Barsch, P. Schwarzbach, S.-P. Luo, H. Junge, M. Beller, S. Lochbrunner, R. Ludwig and A. Brückner, *ACS Catal.,* 2014, **4,** 1845-1849.

75 P. C. Alford, M. J. Cook, A. P. Lewis, G. S. G. McAuliffe, V. Skarda, A. J. Thomson, J. L. Glasper and D. J. Robbins, *J. Chem. Soc., Perkin Trans. 2*, 1985, 705-709.

76 C. E. McCusker and F. N. Castellano, *Inorg. Chem.,* 2013, **52,** 8114-8120.

77 J. R. Lakowicz, Principles of Fluorescence Spectroscopy, 3rd edition, Springer New York, NY, 2006. doi.org/10.1007/978-0-387-46312-4

78 B. Dereka, D. Svechkarev, A. Rosspeintner, A. Aster, M. Lunzer, R. Liska, A. M. Mohs and E. Vauthey, *Nat. Commun.,* 2020, **11,** 1925.

79 E. M. Kober, J. V. Caspar, R. S. Lumpkin and T. J. Meyer, *J. Phys. Chem.,* 1986, **90**, 3722-3734.

80 T. J. Penfold, S. Karlsson, G. Capano, F. A. Lima, J. Rittmann, M. Reinhard, M. H. Rittmann-Frank, O. Braem, E. Baranoff, R. Abela, I. Tavernelli, U. Rothlisberger, C. J. Milne and M. Chergui, *J. Phys. Chem. A*, 2013, **117**, 4591-4601.

81 Y. Leydet, D. M. Bassani, G. Jonusauskas and N. D. McClenaghan, *J. Am. Chem. Soc.*, 2007, **129**, 8688-8689.

82 D. Rehm and A. Weller, *Isr. J. Chem.,* 1970, **8,** 259-271.

83 A. Livoreil, J.-P. Sauvage, N. Armaroli, V. Balzani, L. Flamigni and B. Ventura, *J. Am. Chem. Soc.,* 1997, **119,** 12114-12124.

84 K. L. Cunningham and D. R. McMillin, *Inorg. Chem.,* 1998, **37,** 4114**–**4119.

85 R. Schmidt, C Tanielian, R. Dunsbach and C. Wolff, *J. Photochem. Photobiol., A,* 1994, **79,** 11-17.

86 A. S. Trivella, S. Monadjemi, D. R. Worrall, I. Kirkpatrick, E. Arzoumanian and C. Richard, *J. Photochem. Photobiol., B,* 2014, **130,** 93-101.

87 J. Godard, F. Brégier, P. Arnoux, B. Myrzakhmetov, Y. Champavier, C. Frochot and V. Sol, *ACS Omega,* 2020, **5,** 28264-28272.

88 E. G. Kaye, K. Kailass, O. Sadovski and A. A. Beharry, *ACS Med. Chem. Lett.,* 2021, **12,** 1295-1301.

89 D. T. Payne, J. Hynek, J. Labuta and J. P. Hill, *Phys. Chem. Chem. Phys.,* 2022, **24,** 6146-6154.

90 L. P. Kuhn, R. K. Lutz and C. R. Bauer, *J. Am. Chem. Soc*., 1950, **72**, 5058-5063.

91 R. E. Lutz and S. M. King, *J. Org. Chem.*, 1952, **17**, 1519-1528.

92 E. Altınok, S. Friedle, and S. W. Thomas III, *Macromolecules*, 2013, **46**, 756-762.

93 B. Michelet, C. Deldaele, S. Kajouj, C. Moucheron and G. Evano, *Org. Lett.,* 2017, **19,** 3576-3579.

94 H. Baguia, C. Deldaele, E. Romero, B. Michelet and G. Evano, *Synthesis,* 2018, **50,** 3022-3030.

95 J. Zhang, J.-D. Yang and J.-P. Cheng, *Chem. Sci.,* 2020, **11,** 4786-4790.

96 E. Hasegawa, N. Chiba, T. Takahashi, S. Takizawa, T. Kitayama and T. Suzuki, *Chem. Lett.,* 2004, **33,** 18-19.

97 X.-Q. Zhu, M.-T. Zhang, A. Yu, C.-H. Wang and J.-P. Cheng, *J. Am. Chem. Soc.,* 2008, **130,** 2501-2516.

98 Y. Pellegrin and F. Odobel, *C.R. Chim.,* 2017, **20,** 283-295.

99 C. Minozzi, A. Caron, J.-C. Grenier-Petel, J. Santandrea and S. K. Collins, *Angew. Chem. Int. Ed.,* 2018, **57,** 5477-5481.

100 J. Olmsted and T. J. Meyer, *J. Phys. Chem.,* 1987, **91,** 1649-1655.

101 N. W. Rosemann, P. Chábera, O. Prakash, S. Kaufhold, K. Wärnmark, A. Yartsev and P. Persson, *J. Am. Chem. Soc.,* 2020, **142,** 8565-8569.

102 A. Aydogan, R. E. Bangle, S. de Kreijger, J. C. Dickenson, M. L. Singleton, E. Cauët, A. Cadranel, G. J. Meyer, B. Elias, R. N. Sampaio and L. Troian-Gautier, *Catal. Sci. Technol.,* 2021, **11,** 8037-8051.

103 F. Glaser, C. Kerzig and O. S. Wenger, *Angew. Chem. Int. Ed.,* 2020, **59,** 10266-10284.

Table of content figure for this manuscript:

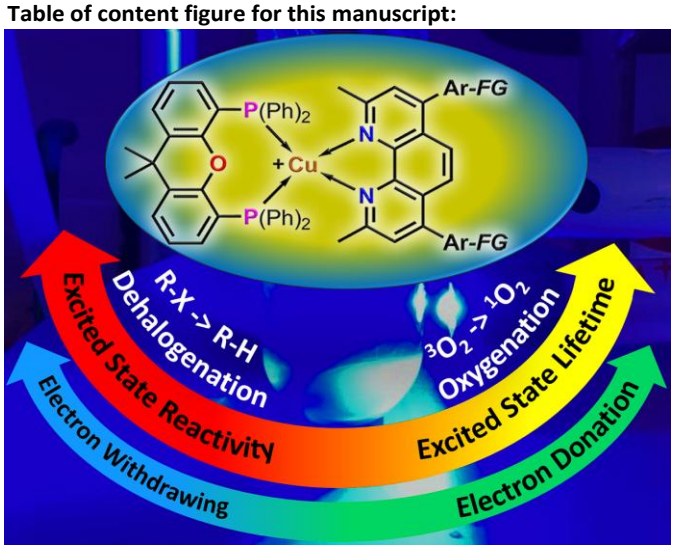

Various electron donating and withdrawing groups and their influence on the structure-property relationships of heteroleptic copper(I) complexes are compared. The results of two different photocatalytic reactions are discussed based on their fundamental photophysical parameters.